Optical Diffusion Tomography With Large Data Sets

Vadim A. Markel, Zheng-Min Wang and John C. Schotland

Departments of Bioengineering and Radiology
University of Pennsylvania, Philadelphia, PA 19104, USA

ABSTRACT

We discuss image reconstruction algorithms for diffuse optical tomography that allow utilization of extremely large data sets. Image reconstruction is performed with experimental data obtained with the use of a CCD camera-based noncontact imager. We demonstrate that more than 10^7 measurements can be acquired and utilized. This is two orders of magintude or more larger than the data sets which are typically used in diffuse optical imaging.

Keywords: Optical tomography, diffusion tomography

1. INTRODUCTION

Optical tomography (OT) is a biomedical imaging modality that utilizes diffuse light as a probe of tissue structure and function.[1] Clinical applications include imaging of breast disease,[2–9] functional neuroimaging [10–17] and small animal imaging.[18] A promising new direction in optical tomography is the use of targeted contrast agents for molecular imaging.[3,18] The physical problem that is considered is to reconstruct the optical properties of an inhomogeneous medium from measurements taken on its surface. In a typical experiment, optical fibers are used for illumination and detection of the transmitted light.[2,19,20] The number of measurements (source-detector pairs) which can be obtained, in practice, varies between $10^2 - 10^4$. A recently proposed alternative to fiber-based experiments is to employ a narrow incident beam for illumination. The beam can be scanned over the surface of the medium while a lens-coupled CCD detects the transmitted light. Using such a "noncontact" method, it is possible to avoid many of the technical difficulties which arise due to fiber-sample interactions.[21,22] In addition, extremely large data sets of 10^8 to 10^{10} measurements can readily be obtained. Data sets of this size have the potential to substantially improve the quality of reconstructed images in OT. As a result, there has been considerable recent interest in the utilization of large data sets in OT.

Reconstruction of images from large data sets is an extremely challenging problem due to the high computational complexity of numerical approaches to the inverse problem in OT. To address this challenge, we have developed analytic methods to solve the inverse problem.[23–25] These methods lead to a dramatic reduction in computational complexity and have been applied in numerical simulations to data sets as large as 10^{10} measurements.[26] Application of these methods to experimental data will be reported elsewhere. Here we discuss the possibility of numerical image reconstruction[27] with data sets of up to $\approx 1.7 \times 10^7$ independent measurements. This number is more than two orders of magnitude larger than what is currently being utilized for image reconstruction.

The advantage of numerical approaches to image reconstruction is their generality. In particular, these methods can be applied to any measurement geometry while the analytic methods require special source-detector arrangement.[23–25] The disadvantage of numerical methods is, however, twofold. First, it is impossible to achieve the same effective level of volume discretization as with analytic methods. Second, the computational

Author e-mails:
V.A.M.: vmarkel@mail.med.upenn.edu
J.C.S.: schotland@seas.upenn.edu
Z.-M.W.: zhengmin@seas.upenn.edu

Photonic Applications in Biosensing and Imaging, edited by Warren C. W. Chan, Kui Yu, Ulrich J. Krull, Richard I. Hornsey, Brian C. Wilson, Robert A. Weersink, Proc. of SPIE Vol. 5969, 59691B, (2005) · 0277-786X/05/$15 · doi: 10.1117/12.628623

complexity, even with the novel developments discussed in this paper, can be significantly larger for numerical methods. Nevertheless, we report here numerical image reconstruction from experimental data with up to 1.7×10^7 independent measurements and with a volume discretization of $\approx 4 \times 10^4$ voxels. The results demonstrate the feasibility of image reconstruction for OT with data sets which are more than two orders of magnitude larger than the current state of the art.

2. MODEL FOR LIGHT PROPAGATION IN TURBID MEDIA

We begin by formulating the model for light propagation in turbid media. We work in the diffusion approximation and assume that the density of electromagnetic energy $u(\mathbf{r})$ obeys the diffusion equation

$$-D\nabla^2 u(\mathbf{r}) + \alpha(\mathbf{r})u(\mathbf{r}) = S(\mathbf{r}) \ , \tag{1}$$

where $\alpha(\mathbf{r})$ is the position-dependent absorption coefficient, $S(\mathbf{r})$ is the power density of a continuous wave source, and D is the diffusion coefficient which is assumed here to be constant. The energy density also obeys the boundary condition

$$\left(u + \ell\hat{\mathbf{n}} \cdot \nabla u\right)\big|_{\mathbf{r}\in\text{boundary}} = 0 \ , \tag{2}$$

on the surface bounding the medium, where $\hat{\mathbf{n}}$ is the unit outward normal and ℓ is the extrapolation distance.[28] The physically measurable specific intensity $I(\mathbf{r}, \hat{\mathbf{s}})$ at the point $\mathbf{r}$ in the direction $\hat{\mathbf{s}}$ is expressed as

$$I(\mathbf{r}, \hat{\mathbf{s}}) = \frac{c}{4\pi}\left(u - \ell^*\hat{\mathbf{s}} \cdot \nabla u\right) \ , \tag{3}$$

This expression can be simplified with the use of (2) if the observation point is on the boundary. Further simplification is achieved when the source is also placed on the boundary. In the slab imaging geometry, when sources are placed on one side of the slab and detectors on the other side, we have

$$I(\mathbf{r}_d, \hat{\mathbf{z}}; \mathbf{r}_s, \hat{\mathbf{z}}) = C_d(\mathbf{r}_d)C_s(\mathbf{r}_s)\left(1 + \ell^*/\ell\right)^2 G(\mathbf{r}_d, \mathbf{r}_s) \ . \tag{4}$$

Here $I(\mathbf{r}_d, \hat{\mathbf{z}}; \mathbf{r}_s, \hat{\mathbf{z}})$ is the specific intensity exiting the medium at the point $\mathbf{r}_d$ in the normal direction $(\hat{\mathbf{z}})$ due to a narrow collimated beam normally entering the medium at point $\mathbf{r}_s$. Note that both $\mathbf{r}_s$ and $\mathbf{r}_d$ are on the medium boundary. The functions $C_d(\mathbf{r}_d)$ and $C_s(\mathbf{r}_s)$ are unknown position-dependent coupling coefficients which may depend on imperfections of the boundary surfaces and properties of the experimental device. $G(\mathbf{r}_d, \mathbf{r}_s)$ is the Green's function of the diffusion equation (1) in an inhomogeneous medium which satisfies

$$\left[-D\nabla^2 + \alpha(\mathbf{r})\right] G(\mathbf{r}, \mathbf{r}') = \delta(\mathbf{r} - \mathbf{r}') \ . \tag{5}$$

Finally, $\ell^* = 3D/c$ is the photon transport mean free path. The unknown constants C_d and C_s can be eliminated from consideration by employing the ratio

$$\frac{I(\mathbf{r}_d, \hat{\mathbf{z}}; \mathbf{r}_s, \hat{\mathbf{z}})}{I_0(\mathbf{r}_d, \hat{\mathbf{z}}; \mathbf{r}_s, \hat{\mathbf{z}})} = \frac{G(\mathbf{r}_d, \mathbf{r}_s)}{G_0(\mathbf{r}_d, \mathbf{r}_s)} \ . \tag{6}$$

Here I_0 is obtained experimentally from transmission measurements in a homogeneous reference medium, while G and G_0 are the corresponding Green's functions obtained analytically from Eq. (1) with position-dependent absorption $\alpha(\mathbf{r})$ in the former case and some reference constant value of absorption α_0 in the latter.

Equation (4) defines a nonlinear problem. We now proceed with linearizatation. To this end, we express $\alpha(\mathbf{r})$ as a sum of a constant known background α_0 and relatively small unknown perturbation $\delta\alpha(\mathbf{r})$. Then the Green's function $G(\mathbf{r}_d, \mathbf{r}_s)$ is given in the mean-field approximation[25] by

$$G(\mathbf{r}_d, \mathbf{r}_s) = \frac{G_0^2(\mathbf{r}_d, \mathbf{r}_s)}{G_0(\mathbf{r}_d, \mathbf{r}_s) + \int G_0(\mathbf{r}_d, \mathbf{r})\delta\alpha(\mathbf{r})G(\mathbf{r}, \mathbf{r}_s)d^3r} \tag{7}$$

Then, we can formulate a linear equation for the unknown function $\delta\alpha(\mathbf{r})$:

$$\int G_0(\mathbf{r}_d, \mathbf{r})\delta\alpha(\mathbf{r})G(\mathbf{r}, \mathbf{r}_s)d^3r = \phi(\mathbf{r}_d, \mathbf{r}_s) \ , \tag{8}$$

where the data function ϕ is related to the experimentally measured transmissions in the inhomogeneous and reference media by

$$\phi(\mathbf{r}_d, \mathbf{r}_s) = G_0(\mathbf{r}_d, \mathbf{r}_s) \left[\frac{I_0(\mathbf{r}_d, \hat{\mathbf{z}}; \mathbf{r}_s, \hat{\mathbf{z}})}{I(\mathbf{r}_d, \hat{\mathbf{z}}; \mathbf{r}_s, \hat{\mathbf{z}})} - 1 \right] \ . \tag{9}$$

In numerical approaches to optical tomography, the integral in (9) is discretized. The result of such discretization is a system of linear equations

$$\Gamma\delta\alpha = \phi \tag{10}$$

This is the main equation which is considered in this paper. Here $\Gamma_{\mathbf{r}_d,\mathbf{r}_s;\mathbf{r}_v} = G_0(\mathbf{r}_d, \mathbf{r}_v)G_0(\mathbf{r}_v, \mathbf{r}_s)$ is an $N \times M$ matrix labeled by the discrete values of the detector and source positions ($\mathbf{r}_d$ and $\mathbf{r}_s$) and the discrete coordinates of the voxels ($\mathbf{r}_v$). The data function ϕ is a vector of the length N which corresponds to the number of measurements (data points) and is labeled by $\mathbf{r}_d$ and $\mathbf{r}_s$.

3. NUMERICAL CONSIDERATIONS

Solving Eq. (10) for $\delta\alpha$ constitutes the linearized inverse problem of OT. It is known to be severely ill-posed. Even if matrix Γ is square, the inverse Γ^{-1} can not be computed numerically because the determinant of Γ is extremely small. Therefore, we will seek the generalized pesudoinverse solution to (10). The latter is based on the SVD of Γ.

In practical image reconstruction, Γ is typically not square. We consider here the case $N \gg M$, i.e., the problem is highly overdetermined. In general, one can expect that over-determining the inverse problem can result in better noise tolerance and better image quality and resolution. This, however, assumes that the noise in all N measurements is statistically independent. In CCD-based measurements, this assumption is physically justified, at least with respect to the noise that originates in the camera itself.

In the case $N > M$, the computational complexity of computing the SVD pesudoinverse of Γ scales as aM^2N+bM^3.[29] Since $N \gg M$, the contribution of the second term is negligible. Therefore, the computational complexity is the same as that of computing the matrix product $\Gamma^*\Gamma$. We will adopt a numerical approach to computing the psudo-inverse based on numerically computing and diagonalizing the $M \times M$ matrix $\Gamma^*\Gamma$. More specifically, the pseudo-inverse solution $\delta\alpha^+$ is given by

$$\delta\alpha^+ = (\Gamma^*\Gamma)^{-1}\Gamma^*\phi. \tag{11}$$

Here $(\Gamma^*\Gamma)^{-1}$ must be appropriately regularized.[30]

The main idea of this paper is that the computation of the pseudo-inverse solution (11) can be potentially simplified without sacrificing the advantages of using large data sets. Indeed, let $F = \Gamma^*\phi$. Computation of F involves one matrix-vector product whose computational complexity is $2MN$ and can be neglected. Computation of the matrix $B = \Gamma^*\Gamma$ requires $2M^2N$ operations. However, we note that B is independent of the experimental noise. All information about the noise is contained in the vector F. Therefore, it is proposed

to compute F exactly using all available data points, but make an approximation for computing B. Namely, let us write a matrix element of B as

$$B_{\mathbf{r}_v,\mathbf{r}'_v} = \sum_{\mathbf{r}_s,\mathbf{r}_d} (\Gamma_{\mathbf{r}_d,\mathbf{r}_s;\mathbf{r}_v})^* \Gamma_{\mathbf{r}_d,\mathbf{r}_s;\mathbf{r}'_v} \ . \tag{12}$$

This summation can be viewed as a discretization of a four-dimensional integral over $d^2r_d d^2r_s$. The precision of the result obtained may not require the same level of discretization of $\mathbf{r}_d$ and $\mathbf{r}_s$ as is required for computing the vector F. Therefore, it is proposed to use *all matrix elements* of Γ for the purpose of computing F, but not all for the purpose of computing B. This would reduce the computational complexity of the most time consuming numerical task, namely that of computing B. At the same time, all N measurements are utilized according to this approach. Note that the proposed method is not equivalent to *binning* of transmission measurements, e.g., averaging of the signal over several adjacent CCD pixels. We, in contrast, use the data from every CCD pixel separately and independently, and take into account the exact coordinate on the measurement surface which corresponds to each particular CCD pixel.

We have implemented the image reconstruction method described above with $\approx 1.7 \cdot 10^7$ experimental data points. The results are discussed in Section 5. We have also validated the method by computing the matrix B directly, without making any approximations. This is a complicated numerical task. We note that the matrix Γ can not be stored in memory as this would require approximately 3,000Gb of memory (assuming $N = 1.7 \cdot 10^7$ and $M = 4 \cdot 10^4$). We have adopted the approach of loading separate blocks each of size $M \times M$ of the matrix Γ in memory. Then the matrix-matrix product B can be repeatedly updated as $B_n = B_{n-1} + \gamma_n^* \gamma_n$, where γ_n is the n-th block and $B_0 = 0$. This numerical procedure can be effectively parallelized. We have used the BLAS level 3 routine SYRK for updating B. This approach proved to be very efficient. On a HP rx4640 server (4x1.6GHz Itanium-II cpus), the sustained speed was approximately 24Gflops.

4. EXPERIMENT

We have constructed a noncontact OT system to test the proposed method of image reconstruction. A schematic of the instrument is shown in Fig. 1. The source is a continuous-wave stabilized diode laser (DL7140-201, Thorlabs) operating at a wavelength of 785 nm with an output power of 70 mW. The laser output is divided into two beams by a beam splitter. The reflected beam is incident on a power meter which monitors the stability of the laser intensity. The transmitted beam passes through a lens onto a pair of galvanometer-controlled mirrors (SCA 750, Lasesys). The mirrors are used to scan the beam, which has a focal spot size of 200μm, in a raster fashion over the surface of the sample. After propagating through the sample, the transmitted light passes through a band-pass interference filter (10LF20-780, Newport) and is imaged onto a front illuminated thermoelectric-cooled 16-bit CCD array (DV435, Andor Technology) using a 23 mm/f1.4 lens. A mechanical shutter is placed in front of the CCD to reduce artifacts associated with frame transfer within the CCD chip. A pulse generator with digital delay is used to trigger and synchronize the CCD, the shutter and the position of the beam.

The sample chamber is a rectangular box of depth 5cm with square faces of area $50 \times 50\text{cm}^2$ constructed of clear acrylic sheets. The beam is scanned on one face of the sample and the opposite face is imaged by the CCD. The chamber is placed equidistantly from the CCD and the laser source along the optical axis at a distance of 110 cm. The chamber is filled with a scattering medium which consists of a suspension of 1% Intralipid in water in which absorbing objects may be suspended.

A tomographic data set is acquired by raster scanning the beam over a 29×29 square lattice with a lattice spacing of 0.5 cm. This yields 841 source positions within a $14 \times 14\text{cm}^2$ area centered on the optical axis. For each source, a 429×429 pixel region of interest is read out from the CCD. This results in 184,041 detectors arranged in a square lattice with an effective lattice spacing equivalent to 0.65mm and all detectors located within a $28 \times 28\text{cm}^2$ area centered on the optical axis. Thus a data set of 1.5×10^8 source-detector pairs is acquired.

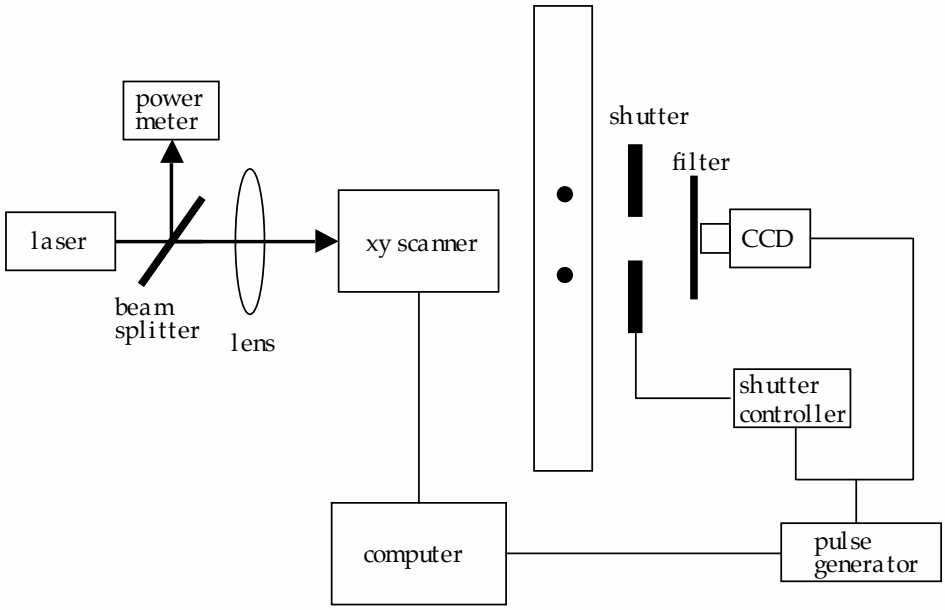

Figure 1. Schematic of the noncontact optical tomography system.

5. RESULTS

We have acquired sets of transmission measurements $I(\mathbf{r}_d, \hat{\mathbf{z}}; \mathbf{r}_s, \hat{\mathbf{z}})$ and $I_0(\mathbf{r}_d, \hat{\mathbf{z}}; \mathbf{r}_s, \hat{\mathbf{z}})$ for two metal balls suspended in the central plain of the imaging chamber. Each ball was 8mm in diameter and painted black. The distance between the ball centers was 30mm.

In order to compute the matrix elements of Γ, as well as the elements of the data vector ϕ according to (9), we need the theoretical expression for the unperturbed Green's function $G_0(\mathbf{r}_d, \mathbf{r}_s)$. The latter is given by

$$G_0(\mathbf{r}_d, \mathbf{r}_s) = \int \frac{d^2q}{(2\pi)^2} \frac{\ell^2 Q(q)}{D} \frac{\exp[i\mathbf{q} \cdot (\mathbf{r}_s - \mathbf{r}_d)]}{[1 + (Q(q)\ell)^2] \sinh[Q(q)L] + 1 Q(q)\ell \cosh[Q(q)L]} \ , \tag{13}$$

where $\mathbf{q}$ is a two-dimensional vector parallel to the slab, L is the slab thickness ($L = 5$cm) for the experimental device described in Section 4) and $Q(q) = \sqrt{q^2 + k_d^2}$. Here $k_d = \sqrt{\alpha_0 / D}$ is the diffuse wave number. Thus, the expression for G_0 contains two constants (ℓ and k_d) which are not known *a priori*. We have found these constants by fitting the theoretical expression (13) to the experimental transmission I_0. The best fit was obtained for $k_d = 0.58\text{cm}^{-1}$ and $\ell = 7$mm. The quality of the fit is illustrated in Fig. 2 in real space. Here we also show the absolute error of the fit.

Once the constants k_d and ℓ were determined, we constructed the matrix Γ and the data vector ϕ and proceeded with image reconstruction. First, we show the result obtained without the approximation discussed in Section 3. Namely, we computed the matrix product $B = \Gamma^* \Gamma$ exactly. However, we have only used such data that corresponds to a transverse source-detector separation of 80 CCD pixels (5.2mm) or less. It can be verified that there is approximately $1.7 \cdot 10^7$ such data points in the experiment described in Section 4. The associated calculation is extremely time-consuming. At the sustained computation speed of 24Gflops, the cpu time required to obtain this reconstruction is approximately 2 weeks. The result is illustrated in Fig. 3. We

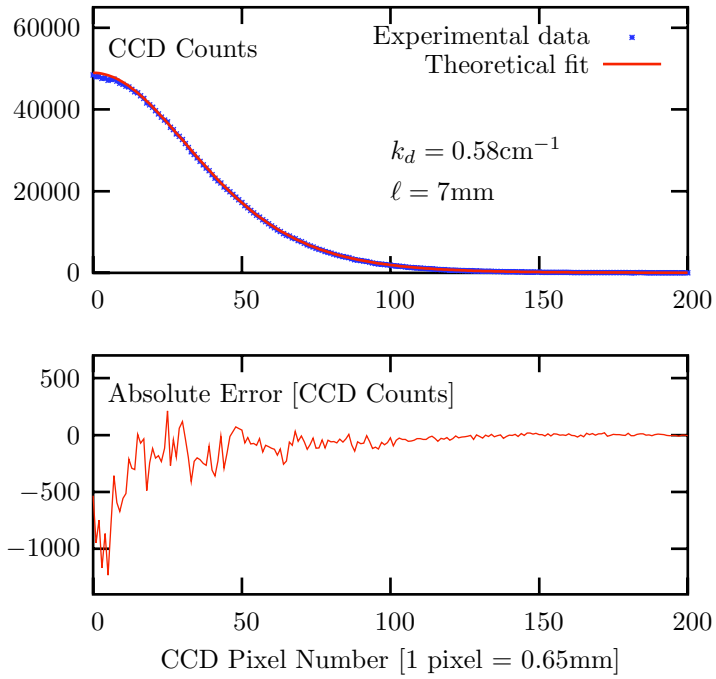

Figure 2. Top: experimental measurements and theoretical fit of the intensity transmitted through a homogeneous slab, as a function of the transverse distance from the point of observation to the axis of the incident narrow beam. Bottom: absolute error.

note that the absorbing objects in the reconstructed image have approximately the same size as the metal balls and are separated by approximately the same distance.

Next, we have used the approximate approach to computing $B = \Gamma^*\Gamma$. Namely, in the summation (12) the lattice of detectors was decimated by the factor n_B. Note that the lattice of sources was left unchanged since the inter-source separation is significantly larger than the inter-detector separation. Here decimation by a factor n means that a sub-lattice of the lattice of detectors is used in the summation, and the period of this sub-lattice is n times the period of the original lattice. Note that decimation by a factor $n_B = 16$ corresponds to reducing the complexity of computing B by a factor of $16^2 = 256$. Also note that the corresponding matrix B was appropriately renormalized in order to keep its trace approximately invariant. The results of such decimations are illustrated in the left column of Fig. 4. We can see that the decimation procedure leaves the quality of the images unchanged.

To further investigate the influence of decimation on the reconstructed images we have also decimated the matrix Γ by a factor n_F for the purpose of calculating the vector $F = \Gamma^*\phi$. The remaining four columns in Fig. 4 illustrate the results of such decimations. Again, the quality of images is virtually unchanged, up to $n_F = 16$. Note that all images in Fig. 4 were obtained at the same level of regularization and are plotted on the same scale.

6. CONCLUSIONS

We have investigated an efficient numerical method for linearized numerical image reconstruction in optical tomography. The method is based on the approximate calculation of the matrix product $\Gamma^*\Gamma$ while calculating the matrix-vector product $\Gamma^*\phi$ exactly, where the quantities Γ and ϕ are defined in Section 2. In the language of tomographic image reconstruction this method can be described as exact calculation of the *backprojection* operation but approximate calculation of the filter. The results obtained indicate that, *at least with the*

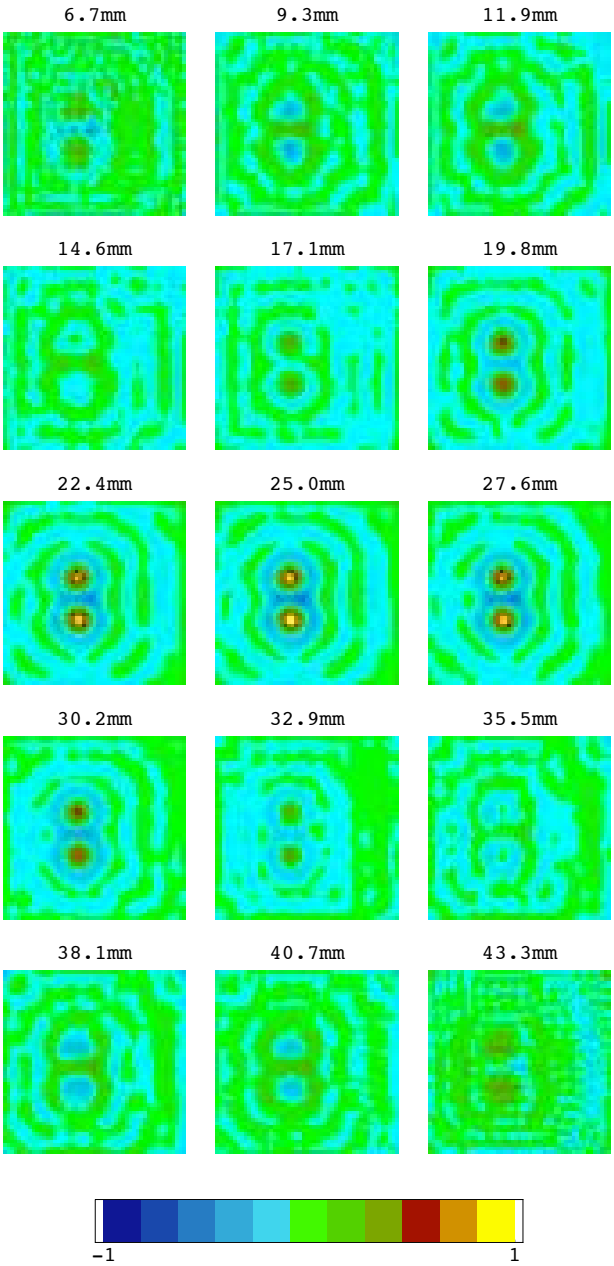

Figure 3. Tomographic slices of the sample. The field of view is 13cm^2 for each slice. The slices are drawn parallel to the slab surface at different distances from the plane of detectors as indicated. A linear color scale is used (see the color bar).

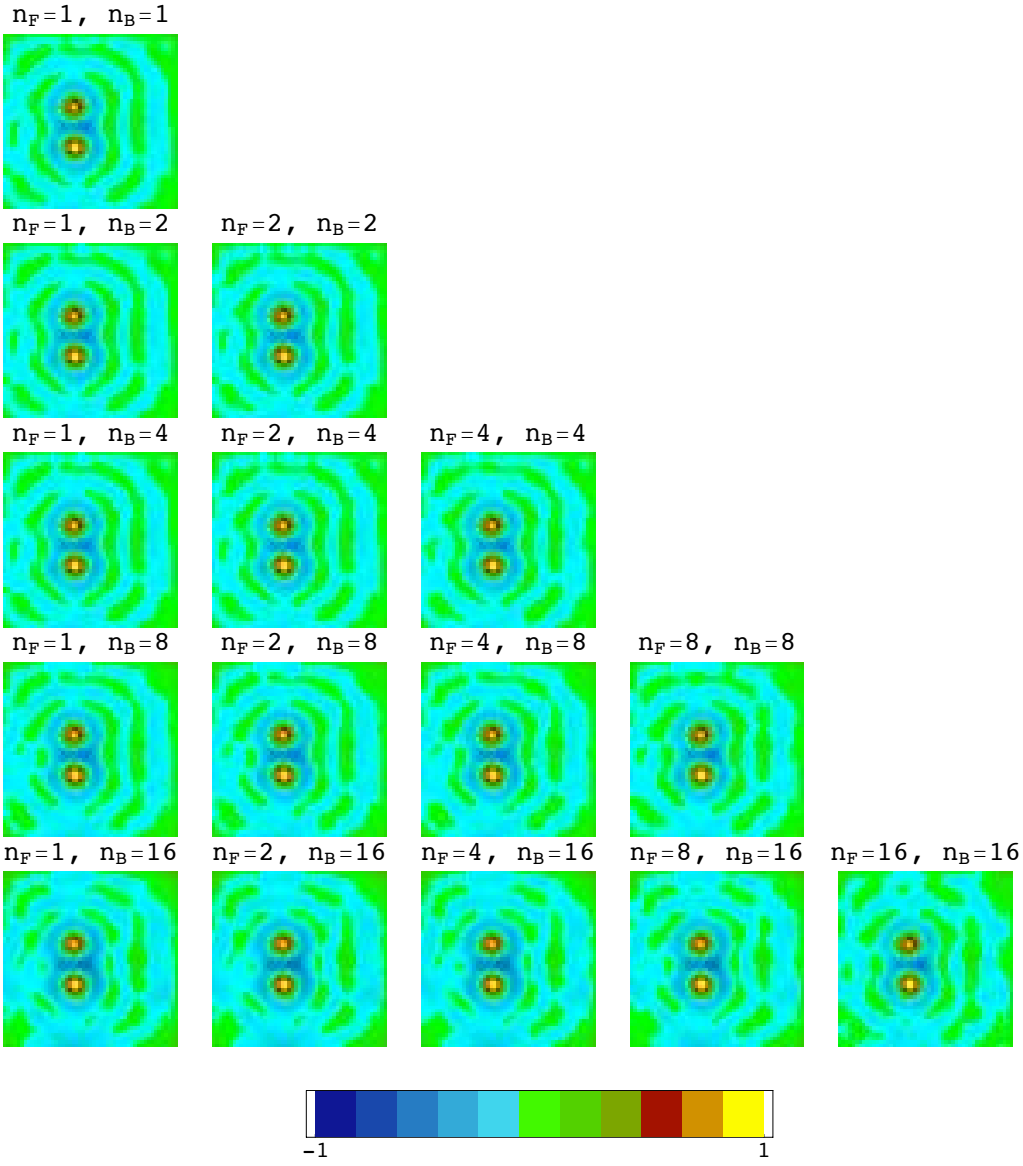

Figure 4. Reconstruction of the central slice corresponding to the depth a of 25mm for different decimation factors n_F and n_B.

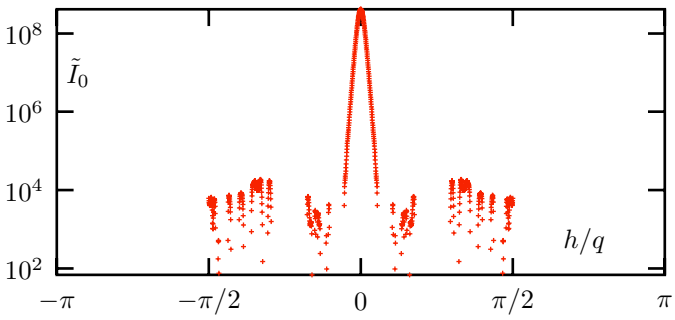

Figure 5. Lattice Fourier transform of the experimental transmission $I_O(\rho)$ for the argument $\mathbf{q}$ on a taken on a fixed line. The period of the detector lattice on which the real space transmission is measured is $h = 0.65$mm. Negative values of $\tilde{I}$ are not shown due to the use of a logarithmic scale.

level of experimental noise present in our measurements, the approximation leaves the image quality virtually unchanged.

We have further seen that image quality does not depend on the decimation factor n_F. Thus, it is not improved when the size of the data set is increased from $\approx 6.6 \cdot 10^4$ (the bottom right plot in Fig. 4) to $\approx 1.7 \cdot 10^7$ (the top left plot in Fig. 4) source-detector pairs. This is, undoubtedly, a consequence of the particular level of noise present in our experimental measurements. The relation between the noise level, the image resolution and the amount of useful data is best revealed by considering the spatial Fourier spectrum of the noise. Consider, for example, the transmission function $I_0(\rho)$ due to a single source which coincides with the optical axis of the system. Here ρ is a two-dimensional vector parallel to the slab surface. Thus, $I_0(\rho)$ is the experimental transmission through a homogeneous reference medium as a function of the transverse source-detector separation. Let $\tilde{I}_0(\mathbf{q})$ be its Fourier transform with respect to the two-dimensional variable ρ. An experimental plot of $\tilde{I}_0(\mathbf{q})$ (for $\mathbf{q}$ taken along a fixed line) is shown in Fig. 5. Here we see a central peak which is relatively noise-free and large-q tails which are dominated by noise. We have found that the critical value of q, above which the noise dominates the signal, is approximately $q_c = 0.15h^{-1}$, where $h = 0.65$mm is the period of the lattice of detectors. This corresponds to a spatial resolution of approximately 12mm which was, indeed, observed in Figs. 3,4. On the other hand, this number indicates that the lattice of sources can be decimated by a factor of $\pi/0.15 \approx 20$ without significant loss of information and, consequently, without significant loss of image quality. Indeed, we have verified that decimation by the factor $n_F = 32$ did result in significant degradation of image quality (data not shown), while decimation with $n_F = 16$ did not.

The limitation encountered in the reconstructed images reported here is specific to our experiment and not fundamental. We have shown using computer-generated data (in the absence of noise) that larger data sets indeed result in better image quality, up to a certain limit.[26] Thus, utilization of large data sets may provide very significant improvements in image quality under different experimental conditions.

Acknowledgments

This research was funded by the NIH under the grants P41RR02305 and R21EB004524. Support from the Whitaker Foundation is also gratefully acknowledged.

REFERENCES

1. A. P. Gibson, J. C. Hebden, and S. R. Arridge, "Recent advances in diffuse optical imaging," *Phys. Med. Biol.* **50**, pp. R1–R43, 2005.
2. S. B. Colak, M. B. van der Mark, G. W. Hooft, J. H. Hoogenraad, E. S. van der Linden, and F. A. Kuijpers, "Clinical optical tomography and nir spectroscopy for breast cancer detection," *IEEE J. Selected Topics in Quantum Electronics* **5**(4), pp. 1143–1158, 1999.

3. D. J. Hawrysz and E. M. Sevick-Muraca, "Developments toward diagnostic breast cancer imaging using near-infrared optical measurements and fluorescent contrast agants," *Neoplasia* **2**(5), pp. 388–417, 2000.
4. Y. Xu, X. J. Gu, L. L. Fajardo, and H. B. Jiang, "In vivo breast imaging with diffuse optical tomography based on higher-order diffusion equations," *Appl. Opt.* **42**(16), pp. 163–3169, 2003.
5. J. P. Culver, R. Choe, M. J. Holboke, L. Zubkov, T. Durduran, A. Slemp, V. Ntziachristos, B. Chance, and A. G. Yodh, "Three-dimensional diffuse optical tomography in the parallel plane transmission geometry: Evaluation of a hybrid frequency domain/continuous wave clinical system for breast imaging," *Med. Phys.* **30**(2), pp. 235–247, 2003.
6. Q. I. Zhu, M. M. Huang, N. G. Chen, K. Zarfos, B. Jagjivan, M. Kane, P. Hedge, and S. H. Kurtzman, "Ultrasound-guided optical tomographic imaging of malignant and benign breast lesions: Initial clinical results of 19 cases," *Neoplasia* **5**(5), pp. 379–388, 2003.
7. X. Intes, J. Ripoll, Y. Chen, S. Nioka, A. G. Yodh, and B. Chance, "In vivo continuous-wave optical breast imaging enhanced with indocyanine green," *Med. Phys.* **30**(6), pp. 1039–1047, 2003.
8. A. Li, E. L. Miller, M. E. Kilmer, T. J. Brukilacchio, T. Chaves, J. Stott, Q. Zhang, T. Wu, M. Chorlton, R. H. Moore, D. B. Kopans, and D. A. Boas, "Tomographic optical breast imaging guided by three-dimensional mammography," *Appl. Opt.* **42**(25), pp. 5181–5190, 2003.
9. S. D. Jiang, B. W. Pogue, T. O. McBride, M. M. Doyley, S. P. Poplack, and K. D. Paulsen, "Near-infrared breast tomography calibration with optoelastic tissue simulating phantoms," *Journal of Electronic Imaging* **12**(4), pp. 613–620, 2003.
10. D. A. Benaron, J. van Houten, D. C. Ho, S. D. Spilman, and D. K. Stevenson, "Imaging neonatal brain injury using light-based optical tomography," *Pediatric Research* **35**(4), pp. A378–A378, 1994.
11. J. P. van Houten, W. F. Cheong, E. L. Kermit, T. R. Machold, D. K. Stevenson, and D. A. Benaron, "Clinical measurement of brain oxygenation and function using light-based optical tomography," *Pediatric Research* **39**(4), pp. 2273–2273, 1996.
12. A. Y. Bluestone, G. Abdoulaev, C. H. Schmitz, R. L. Barbour, and A. H. Hielscher, "Three-dimensional optical tomography of hemodynamics in the human head," *Opt. Express* **9**(6), pp. 272–286, 2001.
13. G. Strangman, D. A. Boas, and J. P. Sutton, "Non-invasive neuroimaging using near-infrared light," *Biological Psychiatry* **52**(7), pp. 679–693, 2002.
14. J. C. Hebden, A. Gibson, R. M. Yusof, N. Everdell, E. M. C. Hillman, D. T. Delpy, S. R. Arridge, T. Austin, J. H. Meek, and J. S. Wyatt, "Three-dimensional optical tomography of the premature infant brain," *Phys. Med. Biol.* **47**(23), pp. 4155–4166, 2002.
15. J. C. Hebden, "Advances in optical imaging of the newborn infant brain," *Psychophysiology* **40**(4), pp. 501–510, 2003.
16. J. P. Culver, A. M. Siegel, J. J. Stott, and D. A. Boas, "Volumetric diffuse optical tomography of brain activity," *Opt. Lett.* **28**(21), pp. 2061–2063, 2003.
17. G. Q. Yu, T. Durduran, D. Furuya, J. H. Greenberg, and A. G. Yodh, "Frequency-domain multiplexing system for in vivo diffuse light measurements of rapid cerebral hemodynamics," *Appl. Opt.* **42**(16), pp. 2931–2939, 2003.
18. R. Weissleder and V. Ntziachristos, "Shedding light onto live molecular targets," *Nature Medicine* **9**(1), p. 123, 2003.
19. F. Schmidt, M. Fry, E. Hillman, J. Hebden, and D. Delpy, "A 32-channel time-resolved instrument for medical optical tomography," *Rev. Sci. Instruments* **71**, p. 256, 2000.
20. T. McBride, B. Pogue, S. Jiang, U. Osterberg, and K. Paulsen, "A parallel-detection frequency-domain near-infrared tomography system for hemoglobin imaging of the breast in vivo," *Rev. Sci. Instruments* **72**, p. 1817, 2001.
21. R. Schulz, J. Ripoll, and V. Ntziachristos, "Noncontact optical tomography of turbid media," *Opt. Lett.* **28**, pp. 1701–1703, 2003.
22. G. Turner, G. Zacharakis, A. Soubret, J. Ripoll, and V. Ntziachristos, "Complete-angle projection diffuse optical tomography by use of early photons," *Opt. Lett.* **30**, pp. 409–411, 2005.
23. J. C. Schotland, "Continuous wave diffusion imaging," *J. Opt. Soc. Am. A* **14**(1), pp. 275–279, 1997.

24. V. A. Markel and J. C. Schotland, "The inverse problem in optical diffusion tomography. ii. inversion with boundary conditions," *J. Opt. Soc. Am. A* **19**(2), pp. 558–566, 2002.
25. V. A. Markel and J. C. Schotland, "Symmetries, inversion formulas and image reconstruction for optical tomography," *Phys. Rev. E* **70**(5), p. 056616(19), 2004.
26. V. A. Markel and J. C. Schotland, "Effects of sampling and limited data in optical tomography," *Appl. Phys. Lett.* **81**(7), pp. 1180–1182, 2002.
27. C. P. Gonatas, M. Ishii, J. S. Leigh, and J. C. Schotland, "Optical diffusion imaging using a direct inversion method," *Phys. Rev. E* **52**(4), pp. 4361–4365, 1995.
28. A. Ishimaru, *Wave propagation and scattering in random media*, Academic Press, San Diego, 1978.
29. G. H. Golub and C. F. Van Loan, *Matrix Computations*, John Hopkins University Press, Baltimore, 1990.
30. F. Natterer, *The mathematics of computerized tomography*, Wiley, New York, 1986.